Journal of Materials Chemistry A

ROYAL SOCIETY OF CHEMISTRY

PERSPECTIVE

View Article Online
View Journal | View Issue

Cite this: J. Mater. Chem. A, 2022, 10, 5863

Single-atom catalysts: stimulating electrochemical CO_2 reduction reaction in the industrial era

Zedong Zhang and Dingsheng Wang *

Carbon monoxide and formic acid play a significant role in industrial processes and are exceedingly economical C_1 products in electrochemical CO_2 reduction reactions (ECR). To improve the yield and catalytic activity in ECR processes, numerous researchers have optimized catalysts and upgraded the electrolyzer. An increase in the electrocatalytic current density and production yield can significantly enable industrial electrochemical conversion from CO_2 to CO/HCOOH. However, the crucial factor restricting the industrialization of ECR is the lack of high-efficiency catalysts. Thus, the development of efficient catalysts for ECR has been ongoing for decades. Traditional nanostructure catalysts suffer from poor product selectivity, unstable structure, and inhomogeneous catalytic active centers, seriously affecting the industrial process. In contrast, single-atom catalysts (SACs) process a uniform coordination environment of active centers, maximum atom-utilization efficiency, and impressive stability, which are suitable as catalysts for industrial ECR. This perspective highlights and summarizes the designed coordination of SACs to obtain a high yield of CO/HCOOH. Moreover, we discuss the fabrication of the electrolyzer and the method of techno-economic assessment (TEA). Finally, we summarize the opportunities and challenges for ECR in industrial processes.

Received 10th September 2021
Accepted 5th November 2021

DOI: 10.1039/d1ta07778c

rsc.li/materials-a

1. Introduction

The continued growth in carbon dioxide emissions has caused ongoing climate change and severe disasters globally.[1] Thus, individual countries plan to peak the CO_2 emission and implement carbon neutrality before the middle of the 21st century, which urgently require the development of carbon capture, storage, and transfer technologies. CO_2 transfer with high efficiencies and low emissions is the holy grail of catalytic chemistry. Traditional thermocatalytic CO_2 reduction is widely used in the industry, which benefits from mature technology and high yield of reduction.[2–4] However, thermocatalysis typically uses hydrogen as the reductant, and the catalytic temperature is high (~573 K). Photocatalytic CO_2 reduction utilizes solar energy exclusively to reduce CO_2 to CO or hydrocarbon fuels with water and photoelectrons.[4] However, its low yield and poor reduction selectivity restricts wide research on CO_2

Department of Chemistry, Tsinghua University, Beijing 100084, P. R. China. E-mail: wangdingsheng@mail.tsinghua.edu.cn

Zedong Zhang received his B.S. Degree from the College of Chemical Engineering at Beijing University of Chemical Technology in 2019. He is now a PhD candidate in Prof. Dingsheng Wang's group in the Department of Chemistry, Tsinghua University. His research interests are focused on the exploration of the relationship between different configurations and the functions of single-atom catalysts.

Dingsheng Wang received his B.S. Degree from the Department of Chemistry and Physics, University of Science and Technology of China in 2004, and his PhD Degree from the Department of Chemistry, Tsinghua University in 2009. He did his Postdoctoral research at the Department of Physics, Tsinghua University. Then, he joined the Faculty of the Department of Chemistry, Tsinghua University in 2012. His research interests focus on the synthesis, structure, and properties of nanomaterials, clusters, and single-atom catalysts.

reduction, and the small reactor sizes limit its extensive application in industry. From the perspective of feedstocks, thermocatalytic CO_2 reduction uses hydrogen as the reductant, whereas photocatalytic and electrocatalytic CO_2 reduction use H_2O/H^+ as the hydrogen source. Considering carbon emission, heat and electricity typically use fossils, which produce more carbon emissions than transfer CO_2, whereas solar or wind energy can realize net-zero carbon emissions. The reactors of thermal and electrical CO_2RR are mature in industry. In conclusion, compared with traditional CO_2 reduction processes (thermal- and photocatalysis), the electrocatalytic CO_2 reduction reaction possess the following characteristics: mature reactor technology in industry, higher yield, safer feedstocks, and the possibility of net-zero carbon emissions. Nowadays, the cost of H_2 feedstock is higher than the revenue gained from CH_4.[2] Accompany with the decrease in the cost of electricity. There has been an increase in the channels to generate electricity (wind, solar, hydroelectric, and nuclear electric energy)[5–9] and in-depth research on highly efficient electrochemical CO_2 reduction (ECR) catalysts.[10,11] Industrial ECR shows apparent advantage in the CO_2 transfer process of storing the electrons in the chemical feedstock. The reduction products of the ECR reaction can be classified into C_1 products and C_{2+} products. Although C_{2+} products are verified to possess higher economic and industrial value, C_1 products typically have higher product selectivity. In this perspective, we focus on the C_1 products that include two-electron products (CO and formic acid, FA) and deeply reduced C_1 products ($8e^-$-process CH_4 and $6e^-$-process CH_3OH). These products possess good selectivity and high energy efficiency (EE).

Single-atom catalysts (SACs) have encouraged intense research in catalytic chemistry.[12–18] Their active centers exhibit a variation in characteristics with a decrease in the size of the metal catalyst. Alternatively, accompanied by a reduction in the size of their active centers, the surface energies of these catalysts can be significantly enhanced. Thus, to overcome this problem, strong coordination ability with substrates can result in the formation of stable catalysts.[19–22] Compared with the traditional nano-dimension catalysts, SACs possess more active catalytic substances with outstanding stability, homogeneous active centers, and higher utilization of metal atoms. The active center of single-atom catalysts is the microscopic atom coordination structure, which is different from nanoparticles. The crystal-lattice effect and defect effect in nanocatalysts affect the selectivity of the ECR products, and the higher surface energy of nanocatalysts result in their aggregation and inactivation. These properties restrict the application of nanoparticles in industry. The strong metal–support interaction (SMSI) of SACs also strengthens the electrons transfer on the catalyst surface. Numerous previous works demonstrated that dispersed Cr, Mn, Fe, Co, Ni, Zn, Pd, Ag, Cd, and Ir SACs prefer reducing CO_2 to CO, and Mo, In, Sn, Sb SACs have been proposed as effective catalysts for FA products.[23,24] Furthermore, they presented an in-depth understanding of the structure–activity relationship of SACs and their optimizations in the ECR process. The Faraday efficiency (FE), current density, energy efficiency (EE), cell voltage (CV), and catalytic stability have gradually become satisfactory to meet the demand of industrial ECR for C_1 products. Among the studies on ECR systems, the electrolyzers have developed from the H-cell to the flow cell and membrane electrode assembly (MEA) electrolyzer. The current density and single-pass conversion have significant improvements, which make the large-scale reduction of CO_2 to C_1 products possible.[25,26]

Techno-economic assessment (TEA) is widely applied to evaluate the economic viability of the ECR process for C_1 products.[27–30] There are many benchmarks to assess, including the revenue from the products, electricity cost, electrolyzer cost, separation consumption, and catalyst cost. The critical factors for catalysts are the catalyst cost, stability, and selectivity in the ECR, which determine where the catalysts cab be scaled up in industry or not.[29] SAC catalysis of ECR usually exhibit excellent C_1 product (CO/FA) selectivity, low cell potential with high EE value, and outstanding catalytic stability as a result of the strong metal–support interaction.[31,32] In this perspective, we mainly focus on the SACs in ECR to produce C_1 products and the challenges in designing and synthesizing effective SACs. Further, we discussed developing an ECR electrolyzer and combining it with traditional TEA methods to predict the possibilities and challenges of SACs in industrial processes (Fig. 1).

2. SACs for simple C_1 products

In general, the catalytic process for $2e^-$ products (from CO_2 to C_1 products, such as CO and FA) involves the following steps: (1) the concentration of CO_2 feedstock; (2) diffusion of CO_2 in electrolyte, and then to the catalytic interface; (3) adsorption and catalytic conversion of CO_2 into *OCHO or *COOH

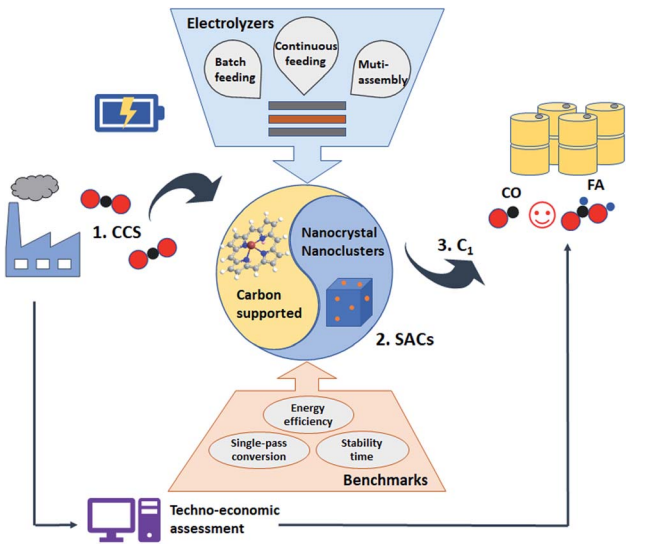

Fig. 1 Schematic of the whole industrial ECR process: the regulation of SACs is the crucial link for transferring CO_2 from carbon capture and storage (CCS) to C_1 products. Multi-assembly electrolyzer scales up the yield of C_1. Through techno-economic assessment of the full lifecycle, the ECR performance satisfies the benchmarks, indicating that SACs are suitable for scaled-up use in industry.

intermediates on the catalyst surface; (4) desorption of oversaturated CO_2 and the C_1 products; and (5) transport of products and collection of redundant CO_2 feedstock. Understanding the structure–activity relationship focuses on the adsorption/desorption steps and the reaction activation energy during the catalytic process. As one of the critical $2e^-$ C_1 products in ECR, CO is commonly associated with carbon-bound intermediates, as shown in Fig. 2, where protons or electrons in the electrolyte induce the metal-catalytic active sites to generate metal* (M*) and adsorb CO_2 to form a carbon-bond (M–C). The intermediates on the catalytic interface are M–*COOH, which further undergo dehydroxylation to CO. The oxygen-bound intermediate theory is used to explain the catalytic process, where FA: M–*OCOH is the key intermediate, which is further converted to FA products through the dihydroxylation mechanism. Surface catalysis of these $2e^-$ C_1 products occurs at single dispersed atomic active centers. Different species of metal elements and the coordination environment of the single dispersed metal atoms are the crucial factors affecting the activity and selectivity in ECR.[33]

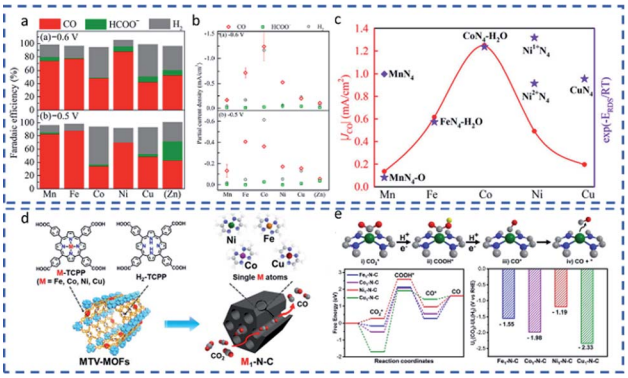

Fig. 3 (a) FE of the MNC catalysts (M = Mn, Fe, Co, Ni, and Cu) at −0.5 V and −0.6 V *vs.* RHE. (b) Volcano trend in partial current densities of MNC catalysts at −0.5 V and −0.6 V *vs.* RHE with the ECR in an H-cell. (c) Experimental CO partial current density and free reaction energy at RDS for MNC catalysts. Reprinted with permission from ref. 45 Copyright 2019, the American Chemical Society. (d) Schematic of the synthesis process of M_1–N–C catalysts (M = Fe, Co, Ni, and Cu) based on MOFs. (e) Free energy diagrams for M_1–N–C catalysts of CO_2 to CO with DFT calculation. Reprinted with permission from ref. 46 Copyright 2020, Wiley-VCH.

2.1. Carbon-supported SACs

Carbon-supported SACs is an essential branch of SACs, which are effective catalysts for ECR. Previous work showed that most carbon-supported SACs with abundant nitrogen-doped are stable activated single-metal ions to form the homogeneous microcosmic structure of M–N_x–C_y. The universal methods for synthesizing carbon-supported SACs include molecular skeleton encapsulation,[34–38] impregnation and pyrolysis,[39–41] coordination regulation,[42–44] and thermal dispersion.

2.1.1. Molecular skeleton encapsulation strategy. The 'molecular skeleton encapsulation strategy' involves the use of porous nanomaterials to encapsulate the metal ions or coordination compounds. Also, through pyrolysis treatment, the metal species can be reduced in the porous nanomaterial substrate. This strategy effectively restricts the agglomeration during heat treatment, where the traditional porous nanomaterials include MOFs, COFs, zeolites, and CNTs. Jaouen *et al.* sacrificed zeolitic imidazolate framework (ZIF-8) as a precursor of N-doped carbon materials.[45] The imidazolate framework was the molecular skeleton to encapsulate different transition metal salts and prepare M–N_X (M = Mn, Fe, Co, Ni, and Cu) SACs through pyrolysis at 1050 °C. They found that all the carbon-supported SACs that exhibited preferable ECR gave particular CO products at −0.5 V and −0.6 V *vs.* RHE (Fig. 3a and b). This research also considered the volcano curve of current density *versus* the atomic number of the transition metal elements. In combination with DFT calculation, the computational reaction activity of the M–N_4 sites shown in Fig. 3c follows the order of FeN_4–H_2O < MnN_4 < $Ni^{2+}N_4$ ≈ CuN_4 < CoN_4–H_2O < $Ni^{1+}N_4$. The tendency of the carbon-supported SACs in ECR can be attributed to the too high *COOH adsorption energy over traditional Mn, Fe, Co-N_4 structures, which increased the side-reaction of the HER (hydrogen evolution reaction). In contrast, Ni, Cu, and Zn-N_4 structures have lower CO_2 adsorption energy, which is conducive to the desorption of C_1 products but at the expense of the active current density of the reaction. Jiang *et al.* used PCN-222 (M-TCPP (M = Fe, Co, Ni, and Cu; TCPP = tetrakis(4-carboxyphenyl)porphyrin)) to encapsulate transition metal atoms with TCPP coordination (Fig. 3d).[46] Carbon-supported SACs were obtained through pyrolysis and removal of the metal Zr. They had a similar conclusion as the previous study, where Ni-N_4 showed a perfect ECR performance compared to the other transition metals (Fig. 3e), which could reach 96.8% FE_{CO} at −0.8 V *vs.* RHE and maintain its stability for 10 h at a current density of −27 mA cm^{-2}. The use of the host–guest interaction of metal–organic framework to encapsulate single atomic sites is a universal method to synthesize various element carbon-supported SACs.[47,48] Zhang *et al.* explored the main group element indium, and the carbon-supported SACs with an In-N_4 moiety exhibited a high probability to produce FA during the ECR.[49] The In-N_4 structure had good stability in the ECR with a reduction in the activity of less than 10% after 60 h and 96% FE_{CO} at 0.65 V *vs.* RHE. However, the strategy of molecular skeleton encapsulation with MOFs suffers from many problems as follows: (1) the metal nodes of the framework are challenging to treat cleanly after pyrolysis or acid etching post-treatment, where single zinc or zirconium atomic sites would affect the

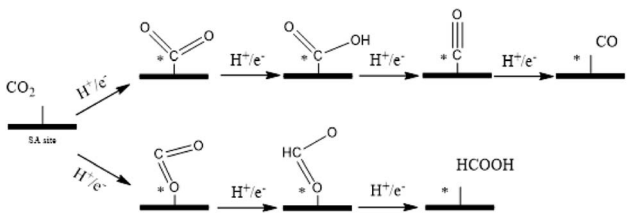

Fig. 2 ECR catalytic pathways of simple C_1 products at the interface. Reprinted with permission from ref. 24 Copyright (2021), The Royal Society of Chemistry.

activity of the reaction.[50,51] Traditional methods of evaporating zinc at high temperatures result in poor reproducibility, which restricts the wide application of carbon-supported SACs in industry. (2) Tube furnaces have a significant deviation at high temperatures, and their energy consumption is too high to produce carbon-supported SACs. Wu *et al.* attempted to clarify the effect of different pyrolyzation temperatures (400 °C, 700 °C, 900 °C, and 1100 °C) on the Fe–N bond states for the ECR process.[52] Compared to the Fe-N_x carbon-supported SACs synthesized at 900 °C, the Fe-N_X carbon-supported SACs synthesized at 1100 °C possessed a higher FE_{CO} but lower current density, which was attributed to the higher temperature reducing the concentration of the iron element. This research also discussed the effect of different temperatures on zinc volatilization and different temperature-induced specific surface areas of carbon-supported SACs. Chen *et al.* regulated the nitrogen species of Fe-N_4 structures by regulating the atmosphere,[53] pyrolysis temperature, and time, wherein the Fe-N_4 system with graphite N had the best FE_{CO} of up to 97% at −0.6 V *vs.* RHE and good stability during the 24 h test under −0.6 V in an H cell. Regulating the microcosmic structure of single atoms and their coordination environment to optimize the conductivity and catalytic activity of carbon-supported SACs can truly guide more theoretical breakthroughs. Alternatively, precise regulation of the coordination environments of carbon-supported SACs lacks a universal synthesis method and enough characterization proof.

2.1.2. Impregnation and coordination regulation strategy. The 'impregnation and coordination regulation strategy' involves the pre-synthetic heteroatom doping of carbon, and then capturing metal atoms through the impregnating and pyrolysis process.[54] This synthetic strategy can solve the problem of miscellaneous metals in the molecular skeleton encapsulation strategy. Zhang *et al.* primarily synthesized N-doped multiwall CNTs, and further mixed them with dicyanamide and manganese acetate.[55] After low-temperature pyrolysis, they obtained Mn–C_3N_4/CNT catalysts with Mn-N_3 moieties. The D-band center models implied that the Mn-N_3 moieties possess a lower density of states (DOS) than the Mn-N_4 moieties (Fig. 4b and c, respectively). Calculation also solved the problem that the Mn-N_4 SACs have a too high *COOH adsorption energy. Single atomic Mn with low coordination numbers shows lower activity energy for the intermediate *COOH, which is beneficial to obtain C_1 products in the ECR. It also could keep the FE_{CO} above 90% for 20 h under −0.55 V *vs.* RHE in an H-cell. Furthermore, the current density reached 15 mA cm^{-2} (Fig. 4a). Carbon-supported SACs with a hierarchical structure, enormous surface area, and hole capacity can effectively induce the contact between the active centers and the reactant.[34,35] Li *et al.* used the hard-template method, as shown in Fig. 4d, to polymerize a nitrogen-containing polymer (melamine-resorcinol-formaldehyde polymer) over SiO_2 nanospheres.[56] After pyrolysis and etching treatments, the hierarchical N-doped carbon shell was further loaded with cobalt peptides to obtain SACs with Co-N_5 moieties. The comparative tests in the H-cell showed that this supported molecular catalyst had a higher current density and FE_{CO} than conventional homogeneous molecular catalysts (Fig. 4e). Supported molecular catalysts are different from the common carbon-supported SACs obtained through pyrolysis, which have homogenous active center sites and can effectively avoid the differences in selectivity and reproducibility caused by the unevenness of the atomic structures. Nitrogen atoms stabilize the molecular catalyst on the carbon support to form a carbon-supported single-atom catalyst with M-N_x moieties. The coordination numbers of the metallic centers are always more prominent than the original molecular catalysts. This is a typical type of coordination regulation strategy. Conversely, the stability of carbon-supported SACs should be considered without heat treatment, *i.e.*, whether the molecular catalysts would change during the catalytic process. Liang *et al.* used the coordination regulation method to load peptide nitride (NiPc) structures regulated by different functional groups (–H, –CN, and –OMe) on the sidewalls of CNTs.[57] The CNTs modified with NiPc–OMe exhibited outstanding FE_{CO} and stability in the ECR test. Other functional groups (–H and –CN) were verified to increase the electron density of the nickel centers, which weakened the desorption of CO and affected the subsequent catalytic reaction.

2.1.3. Thermal dispersion strategy. The thermal dispersion method, which involves reducing nanoparticles at high temperature to release metal atoms on N-doped carbon materials, is a type of synthetic method with significant industrial prospect. A milestone was achieved in the study that showed that a 2 nm Pd nanoparticle could disperse into Pd single atoms during the carbonization of ZIF-8.[58] Initially, Ostwald ripening occurs the early stages of medium-temperature carbonization, causing the size of the Pd particle to increase to about 5 nm. With an increase in temperature, zinc is evaporated from the previous position, which prompts the Pd single atoms to be released. Metallic zinc is convenient to form Pd–Zn bonds[59] and Pt–Zn bonds,[60] and thus the evaporation of zinc could drive the dispersion of Pd or Pt nanoparticles at high temperature. Another universal method to convert nanoparticles into single

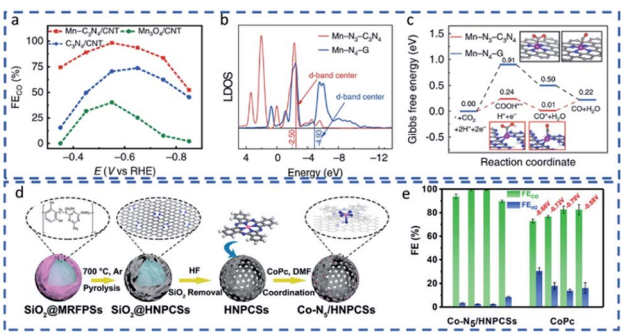

Fig. 4 (a) FE_{CO} of the catalysts with an Mn-N_3 moiety and Mn_3O_4 nanoparticles at different reduction potentials. (b) DFT calculation results for local density of states (LDOS) of Mn active centers in different SACs. (c) Calculated free energy diagrams on Mn-N_3 and Mn-N_4 moieties in ECR to produce CO. Reprinted with permission from ref. 55 Copyright 2020, Springer Nature. (d) Schematic of the synthesis of SACs with a Co-N_5 moiety. (e) FE_{CO} of the Co-N_5 moiety and CoPc with an H-cell. Reprinted with permission from ref. 56 Copyright 2018, the American Chemical Society.

atoms is the use of a reducing atmosphere (NH_3 and H_2) to induce the evaporation of nanoparticles and transfer single atoms to the N-sites of the carbon support.[61–63] Li *et al.* utilized dicyanamide to produce ammonia and promote the conversion of bismuth nanoparticles to Bi-N_4 moieties.[64] This Bi-N_4 catalyst exhibited 97% FE_{CO} under −0.5 V *vs.* RHE in the H-cell test.

In summary, the strategies for the synthesis of carbon-supported SACs can be classified into the four above-mentioned categories. The molecular skeleton encapsulation method is commonly used in specific mesoporous carbon materials (MOFs,[65] COFs,[66] HOFs, *etc.*). The advantage of this method is that it can be universally employed to synthesize carbon-supported SACs with different elements (Mn, Fe, Co, Ni, Cu, Zn, Ag,[67] Cd,[68] In, Sn,[69,70] Sb,[71] and Bi), which show superior performances to produce C_1 products in ECR. However, carbon-supported SACs obtained with this method often suffer from inhomogeneous active centers and poor reproducibility. These disadvantages restrict their large-scale application in industry. Impregnation and pyrolysis is a method to load single-metal atoms following pre-synthetic heteroatom doping of the carbon substrate. The metal sites do not require high-temperature treatment for this method. The coordination regulation method can be employed to design the structure of substrates and preciously synthesize homogenous carbon-supported SACs. Both the impregnation and pyrolysis methods and coordination regulation methods can be employed to fabricate SACs with a more obvious microcosmic structure and produce carbon-supported SACs on the gram-scale, which is beneficial for industrial ECR. The thermal dispersion method is a novel notion of recovering the disabled nanoparticle catalysts as efficient carbon-supported SACs.[72] However, there is still a lack of research on the dispersion mechanism and the size and capacity limits of nanoparticles.

2.2. Nanocrystal/cluster-supported SACs

2.2.1. The synthetic methods. Nanocrystal catalysts have specific lattices and defect effects. Single-metal atoms anchored on different lattices or defects can regulate the selectivity of the products. Different from the characteristics of inert carbon substrates, nanocrystals typically have high catalytic activity, which modify the single metallic atoms at the interface and can regulate the local electron density at the active centers.[73–78] The impregnation method is a general strategy to synthesize nanocrystal/cluster-supported SACs, which is different from carbon-supported SACs, where galvanic replacement (GR)[79,80] and cation/anion exchange reaction[81,82] can occur on nanocrystals/clusters. Zheng *et al.* developed a method to deposit single Pd atoms on the (100) and (110) facets of Cu nanocrystals through a GR reaction.[83] Their different catalytic performances provide advanced perception for synthesizing nanocrystal-supported SACs. Sargent *et al.* synthesized Cu nanoparticles with single-dispersed gold atoms on their surface, which could effectively convert CO_2 to C_2 products in a flow cell.[84] Cu nanomaterials are widely used to produce C_{2+} in ECR. Single metallic atom-doped Cu nanoparticles can regulate the selectivity of C_{2+} products. Cation exchange reaction (CER) methods were previously applied for the synthesis of intermetallic compounds with specific proportions. Li's group use the CER method to synthesize Pt single atomic site Cu_2S catalysts.[85] However, there are only a few studies on the synthesis of nanocrystal-supported SACs and their application in the ECR reaction. Under the guidance of theory, Li *et al.* found that Au nanoparticles loaded on defective CeO_2 spontaneously dispersed into Au atoms at high temperature.[86] Inspired by this, Wang *et al.* synthesized Ag nanoparticles/MnO_2 nanorods and converted them to Ag single-atomic sites/MnO_2 (Fig. 5a).[87] This Ag SAs/MnO_2 possessed high CO product selectivity in the ECR (FE_{CO} of up to 95.7% at −0.85 V *vs.* RHE, and the current density was nearly 6 mA cm^{-2} in the H-cell) and good catalytic stability for 9 h at −0.85 V. A more common method for the preparation of nanocrystal/cluster-supported SACs is the "one-pot" strategy. Yao's group mixed metal salts precursors with an Fe/Au atomic ratio of 1 : 19 and reduced them to Fe_1/Au single-atom alloy catalysts *via* a "one-pot" method.[88] This material was shown to possess high activity and selectivity in the ECR for CO products. Single-atom Fe doping also amplified the mass-specific activity to 399 mA mg^{-1}, which is much higher than that of pure Au nanoparticles (Fig. 5b–d). Jiao *et al.* added a Cd salt precursor during the fabrication of thiolate-protected Au nanoclusters ($Au_n(SR)_m$) and achieved single-atomic Cd dispersed gold nanoclusters (Fig. 5e).[89] This regulation improved the FE_{CO} and current density to yield C_1 products (Fig. 5f). Unsatisfactorily, the modification of inexpensive metal elements on noble metal nanomaterials has not reduced catalyst cost, which restricts

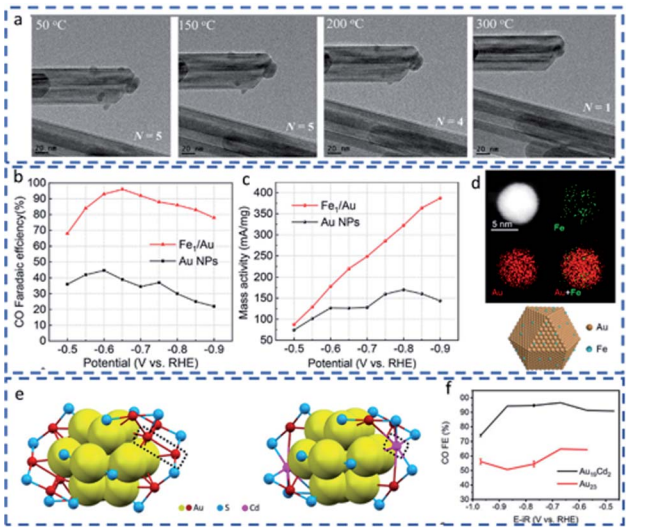

Fig. 5 (a) *In situ* AC-TEM monitoring of the Ag nanoparticle thermal dispersion phenomenon to fabricate Ag-SA/MnO_2. Reprinted with permission from ref. 87 Copyright 2021, Wiley-VCH. (b) FE_{CO} of the Fe_1/Au SAA and Au nanoparticle catalyst at different reduction potentials. (c) Mass activity of Fe_1/Au and Au nanoparticle catalyst at different reduction potentials in ECR. (d) Schematic diagram and EDS mapping figures of Fe_1/Au. Reprinted with permission from ref. 88 Copyright 2021, the American Chemical Society. (e) Schematic diagram of Cd_2Au_{19} and Au_{23} nanocluster catalysts. (f) FE_{CO} of the Cd_2Au_{19} and Au_{23} nanocluster catalysts. Reprinted with permission from ref. 89 Copyright 2021, Wiley-VCH.

their application in industry. Reducing the dosage of noble metals and anchoring noble metal atoms on transition metals is more beneficial for the practical application of SACs. Cao *et al.* used the molecular skeleton encapsulation method to synthesize Ni nanoclusters with single-dispersed Zn atoms. Although this method provides different types of active centers, it is also profitable to explore whether modifying the metal atoms on the nanocrystals/clusters could optimize the stability and activity performance in the ECR.

2.2.2. The perspective of nanocrystal/cluster-supported SACs. Currently, the synthesis of nanocrystal/cluster-supported SACs is still a novel field for effectively electrically reducing CO_2 to simple C_1 products. SACs suffer from a common problem, where the number of active sites is always too low to obtain high catalytic activity in many fields.[90–93] Many studies indicate that SACs possess outstanding turnover frequency (TOF). However, their low yield (compared to commercial catalysts, at the same volume/quality) impedes the scale-up of the catalytic process. Nanocrystals and nanoclusters have high catalytic activities and specific nanosize effects. Transition metals are inexpensive with abundant reserves, and thus these elements can be effectively utilized to synthesize nanomaterials. Nobel metals exhibit unique catalytic performances when downsized to the atomic level, promoting the catalytic selectivity of transition metals. Combining single noble metal atoms and transition metal nanomaterials can be employed to optimize the synthesis of efficient SACs. Inspired by the development of nanocrystals, the strategies for the synthesis of nanocrystal/cluster-supported SACs in the future mainly include "one-pot" and "multi-steps" methods. The "one-pot" method is easy for the preparation of SACs. However, more metal atoms are assembled in the interior, which causes the atomic utilization of noble metal to be lower than 100%. The "multi-step" method is normally employed to fabricate nanomaterials initially, and GR, CER and nanoparticle conversion reactions are employed to synthesize SACs. Nobel metal atoms can be effectively anchored at the catalytic interface with the "multi-step" method, and thus the atomic utilization of noble metal elements is nearly 100% (Table 1).

3. SACs for deeply reduced C_1 products

Deeply reduced C_1 products initially include the $8e^-$-transfer product methane and $6e^-$-transfer product methanol. The catalytic mechanism is the same as that to obtain simple C_1 products. Metal–carbon or metal–oxygen intermediates are formed on the single atomic site, and there is no C–C coupling process. Alternatively, deeply reduced C_1 products need more electrons to reduce the $2e^-$ products (CO and FA). Currently, the consensus is that after the $2e^-$ reduction process, the *CO intermediate is preferentially reduced by protons/electrons to *CHO and *OCH intermediates rather than desorbed to produce CO (Fig. 6).[33,94–96] Catalytically, the formation of the *CHO intermediate and *OCH is the rate-determination step in producing CH_4 and CH_3OH. Therefore, regulation of the adsorption energy of the *CO intermediate is the key to catalyzing deeply reduced C_1 products.[97]

Zheng *et al.* synthesized Cu single-dispersed CeO_2 structures *via* the impregnation and pyrolysis method,[98] where Cu single atoms were trapped in the defects of CeO_2 through exchange of the valence of Ce^{4+} and Ce^{3+}, presenting the oxidation of +1 (Fig. 7a). In the ECR test with an H-cell, the Cu-SA/CeO_2 catalyst showed a notable FE_{CH4} of 58% at −1.8 V *vs.* RHE, and the current density reached 70 mA cm^{-2} simultaneously (Fig. 7b). The synergistic effect of Cu single atoms and the substrate promotes the adsorption stability of the CO intermediate. Single-dispersed copper atoms suppress the occurrence of C–C coupling, and thus Cu-SA/CeO_2 catalysts can efficiently produce the deeply reduced product. Xin *et al.* used the coordination regulation and pyrolysis method for the synthesis of a carbon-supported SAC with a Zn-N_4–C moiety.[99] In 1 M $KHCO_3$, this catalyst exhibited 85% FE_{CH4} with a current density of 31.8 mA cm^{-2} (Fig. 7c and d) and stability for 35 h without an obviously decrease at a reduction potential of −1.8 V. In the $6e^-$-transfer production of methanol, as the competition product of CH_4, the rate-determination step (RDS) of the ECR process is the formation of the metal–oxygen intermediate, which requires the regulation the *CO adsorption energy. Han *et al.* synthesized a defected CuO structure with Sn single atoms using H_2 plasma-treated CuO to produce oxygen defects and trapped Sn atoms.[100] This catalyst showed good selectivity for methanol in CO_2-saturated ionic liquid (nearly 88.6% FE for methanol at −2.0 V). A peptide nitrile cobalt (CoPc) was also found to convert CO_2 to methanol after loading CNT. Liang *et al.* modified the peptide nitrile with amidogen (CoPc–NH_2) and loaded CoPc–NH_2 on CNT the substrate.[101] The FE for methanol could reach 44% at the beginning of ECR at −1.0 V *vs.* RHE and the largest partial current density of 10.6 mA cm^{-2} was observed for the CoPc–NH_2/CNT catalyst. There is also a lack of research exploring the relation between SACs and the deeply reduced C_1 product. Most reports indicate that the single-dispersed atom sites block the transition state of C–C coupling. According to the Sabatier principle, regulating the adsorption energy of *CO on the active center can selectively produce $2e^-$, $6e^-$ or $8e^-$ products. However, the deeply reduced C_1 products face the challenges of low catalytic activity, poor stability, and impaired conversion, which should be promoted in the future.

4. Development of ECR electrolyzers

In the development of ECR, the design of the electrolyzer has pushed the lab-scale electric reduction of CO_2 towards large-current and yield industrial-scale. The design of ECR electrolyzers mainly focuses on the following aspects: (1) effectively separating the products of the cathode and anode and preventing the reduction products of ECR oxidation at the anode. The crossover effect is deemed initially to decrease the reduction efficiency in the ECR. (2) Increasing the solubility and mass transfer rate of CO_2. (3) Reducing the ohmic loss of the electrolyzer and the instantaneous volatility of local pH, which decrease the EE of electrolyzers. (4) Promoting the exchange and separation of products and continuous CO_2 conversion.

Table 1 Summary of the performance of different SACs in the ECR

Catalyst	Mass loading (mg cm^{-2})	Electrolyte	Product	Reductionpotential (V *vs.* RHE)	FE (%)	TOF (h^{-1})	Current density (mA cm^{-2})	Cell	Stability time (h)	Reference DOI
Ag_1-N_3/PCNC	—	0.1 M $KHCO_3$	CO	−0.37	95	∼1000	7.6	H cell	10	10.1021/acsami.1c03638
Ni_1–N–C	0.53	0.5 M $KHCO_{33}$	CO	−0.80	96.8	11 315	27	H cell	10	10.1002/anie.202008787
Fe–N–C	0.40	0.1 M $KHCO_3$	CO	−0.728	95.3	∼2700	∼8.4	H cell	10	10.1002/anie.202012329
In-N_4–C	—	0.5 M $KHCO_3$	HCOOH	−0.95	96	12 500	8.87	H cell	60	10.1002/anie.202010903
Cd-NC	1.5	0.5 M $KHCO_3$	CO	−0.728	91.4	—	∼5	H cell	10	10.1021/acs.nanolett.1c00432
FeN_4/graphitic N	—	0.1 M $KHCO_3$	CO	−0.60	97	—	6.87	H cell	24	10.1016/j.chempr.2021.02.001
Sb-N_4	0.102	0.5 M $KHCO_3$	HCOOH	−0.8	94	—	∼4	H cell	10	10.1039/D0EE01486A
CoN_5–C	—	0.2 M $NaHCO_3$	CO	−0.79	99.4	480.2	6.2	H cell	10	10.1021/jacs.8b00814
Bi-N_4	—	0.1 M $NaHCO_3$	CO	−0.5	97	5535	3.9	H cell	4	10.1021/jacs.9b08259
Ni-SA/NC	3.00	1 M KOH	CO	−1.06	96.9 (0.66 V)	2187	213.2	Flow cell	20 (H cell)	10.1016/j.nanoen.2020.105689
Mn-N_3–C	1.00	[Bmim]BF_4/CH_3CN–H_2O	CO	−0.55	98.8	—	22.7	H cell	20	10.1038/s41467-020-18143-y
Ni-Pc	0.05	1.0 M $KHCO_3$	CO	−0.61	99.5	43 200	400	MEA	40	10.1038/s41560-020-0667-9
Cu/Ni$(OH)_2$	1	0.5 M $KHCO_3$	CO	−0.50	92	11 315	∼6	H cell	22	10.1126/sciadv.1701069
$Cu_{20}Sn_1$	0.57	0.5 M $KHCO_3$	CO	−1.0	95.3	—	12.5	H cell	10	10.1021/acscatal.1c02556
Cu_1Sn_1	0.57	0.5 M $KHCO_3$	HCOOH	−1.2	95.4	—	24.1	H cell	10	
Pd_4Ag	1	0.1 M $KHCO_3$	HCOOH	−0.23	94	—	5	H cell	1h	10.1002/adma.202005821
$Au_{19}Cd_2(SR)_{16}$	0.02	0.5 M $KHCO_3$	CO	−0.60	90	—	45	H cell	—	10.1002/anie.202016129
Ag_1/MnO_2	—	0.5 M $KHCO_3$	CO	−0.85	95.7	—	∼4	H cell	9	10.1039/D0EE01486A
Fe_1/Au	0.1	0.5M $KHCO_3$	CO	−0.9	96.3	11 521	17.5	H cell	4	10.1021/acs.nanolett.0c04291
Cu/CeO_2	—	0.1 M $KHCO_3$	CH_4	−1.8 V	58	—	56	H cell	2	10.1021/acscatal.8b01014
Cu-N_2	1	0.1 M $KHCO_3$	C_2H_4	−1.4	24.8	—	6.84	H cell	10 h	10.1021/acsenergylett.0c00018
Cu-N_4	1	0.1 M $KHCO_3$	CH_4	−1.4	13.9	—	3.83	H cell	10 h	
Zn-N_4	0.4	1 M $KHCO_3$	CH_4	−1.8 (V *vs.* SCE)	85%	—	39.9	H cell	35 h	10.1021/jacs.9b12111

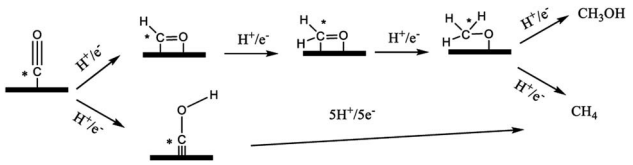

Fig. 6 ECR catalytic pathways for deeply reduced C_1 products at the catalytic interface.

According to the feedstock and separation function of electrolyzers, we can divide the electrolyzers into the batch, semi-batch, and continuous electrolyzers.[102]

4.1. Batch or continuous electrolyzers

Batch and semi-batch electrolyzers mainly refer to single-compartment and double-membrane electrolyzers (H-cell). The products need to be separated from the reaction system after the reaction each time. The primary issue associated with single-compartment electrolyzers is the crossover effect, which oxidizes the C_1 products to CO_2 and reduces the yield. The H-cell, which separates the cathode and anode with an ion-exchange membrane, can efficiently decrease this crossover effect. However, the anion-exchange membrane (AEM) also causes crossover in alkali electrolytes after long-time ECR catalysis.[103] The H-cell possesses a simple operation process, which is suitable for lab-scale research. The CO_2 at the cathode normally encounters low saturation, which reduces the contact between the reactant and active catalytic centers. The inferior fluidity of electrolytes induces a poor mass transfer rate and restricts the increase in the current density of ECR. The OER product at the anode is mixed with CO_2 or CO, which decreases the purity of the gaseous C_1 product, and the waste O_2 results in a decrease in the EE of the electrolyzer.[104]

Zhang *et al.* proposed a solution to this problem. They used Cl^- to react at the anode and collected NaClO product.[105] The

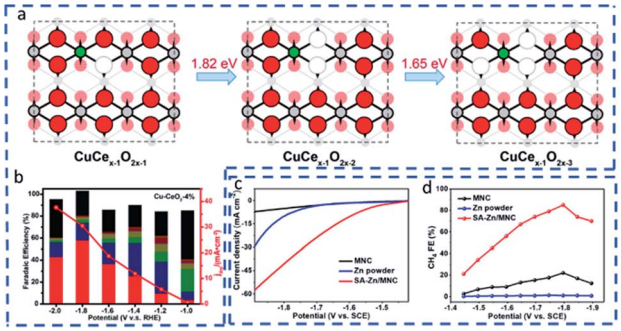

Fig. 7 (a) Stable structure model for Cu-SA/CeO_2 catalysts from DFT calculations. (b) FE_{CO} of the Cu-SA/CeO_2 catalysts at different reduction potentials (red columns represent CH_4 and brown columns represent H_2). Reprinted with permission from ref. 98 Copyright 2018, the American Chemical Society. (c) Linear sweep voltammetry curves of Zn-N_4–C in ECR. (d) FE_{CH4} of Zn-N_4–C SACs at different reduction potentials. Reprinted with permission from ref. 99 Copyright 2020, the American Chemical Society.

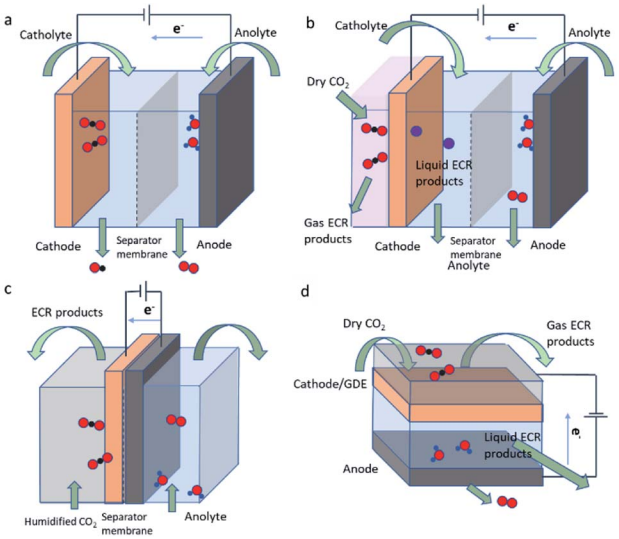

Fig. 8 Schematic diagram model for different flow-cell configurations: (a) liquid-fed flow cell, (b) liquid-fed flow cell with the gas chamber, (c) vapor-fed flow cell, and (d) microfluidic flow cell.

CO_2 reactant was electrically reduced on the Fe-N_x moiety SACs to produce CO and Cl^- oxidized on RuO_2 to produce ClO^-, where the whole electrolyzer possessed 96% FE_{CO} and 82% EE, significantly improving the EE compared to the OER wasted on the IrO_2 anode. However, batch and semi-batch electrolyzers are unsuitable for the efficient and continuous utilization of CO_2 feedstock. Accordingly, the establishment of constant feeding and separation devices is the development trend of electrolyzers. Continuous electrolyzers should accelerate the fluidity of electrolytes, and consecutive feeding of CO_2 can also facilitate the mass transfer and reduction in current density. The flow cell is a type of ordinary continuous electrolyzer, which can be divided into liquid-fed, vapor-fed, and microfluidic flow cells.[106–108] The liquid-fed flow cell cathode and anode are separated by an electrolyte and often include a liquid cell and gas–liquid cell. Both humidified CO_2 and dry CO_2 can generate the reduction products on the cathode (Fig. 8a). The mass transfer is faster than batch electrolyzers. However, the considerable distance between the cathode and anode causes ohmic loss, and higher partial pressure of CO_2 produces a decrease in conductivity near the electrode. Thomas F. Jaramillo's group designed a liquid-fed flow cell with dry CO_2 as the feedstock,[109] which has a liquid volume of 8 mL and a gas volume of 3 mL and can obtain 25 reduction products in the ECR. This forms the prototype for the flow cell design (Fig. 8b). One of the potential solutions for reducing the ohmic loss is to decrease the distance between both electrodes. The vapor-fed flow cell is characterized by a minimum distance between electrode plates with lower ohmic loss, but the requirements for the separator membrane are much more demanding. Vapor-fed flow cells initially use humidified CO_2 as the feedstock and have the desired mass-transfer rate and current density in the ECR. However, the ion-exchange membrane needs to withstand extreme current conditions. To date, the exploration of separator membranes with high intensity and ion selectivity is still a considerable challenge. The liquid-products in vapor-fed flow cells (Fig. 8c) diffuse slowly, which can cause the separator and SACs to be deactivated. Thus, third-generation microfluidic flow cells were designed (Fig. 8d), where there is a thin layer of flowing liquid between the cathode and the anode to transfer the liquid products. Dry or humidified CO_2 rapidly contacts the SACs on the gas diffusion electrode (GDE), and the accelerated mass transfer also enhances the current density. The microfluidic flow cell is widely used in ECR tests, where dry CO_2 contacts with superhydrophobic gas diffusion electrodes to produce C_1 products. The advantage is that the gas and liquid can be partially separated by different electrolytic cells. However, achieving a uniform SAC coating on the GDE and the hydrophilic leakage of the GDE caused by the reduction voltage and alkaline environment are still challenges for further exploration.[110]

4.2. MEA electrolyzers and multi-assembly electrolyzers

Accompanying the development of electrolyzers, the current density of ECR has a noticeable improvement, gradually increasing the production scale of ECR from lab-scale to pilot-plants. However, it is difficult to achieve an ideal single-pass conversion rate of CO_2 with a traditional single electrolyzer. C. Janáky *et al.* designed a multi-assembly flow cell based on the microfluidic flow cell, which improved the single-pass conversion by extending the transfer distance of CO_2 molecules.[111] As shown in Fig. 9a, dry CO_2 was primarily treated to obtain humidity and pressure CO_2 feedstock. The feedstock was bubbled into the multi-assembly flow cell. The current density for the production of CO products reached 250 mA cm^{-2} under normal pressure. In the 10 bar-pressurized ECR test, the current density reached up to 300 mA cm^{-2} with 95% FE_{CO} and the CO_2 single-pass conversion of this multi-assembly flow cell was nearly 40%. The CO product demonstrates its potential for the industrialization of the ECR. A further development of the electrolyzer is membrane electrode assembly (MEA) devices

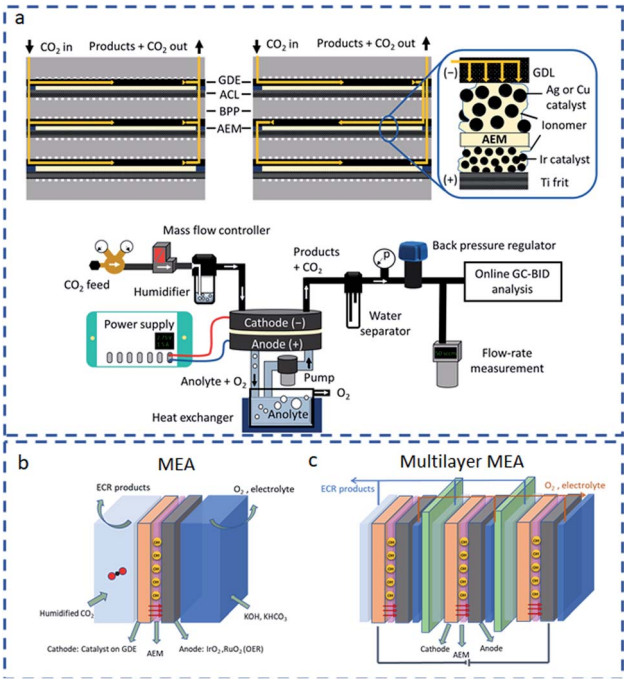

Fig. 9 (a) Schematic flowchart of multilayer electrolyzer and serial configurations. Reprinted with permission from ref. 111 Copyright 2020, the American Chemical Society. (b) Schematic diagram of MEA electrolyzer structure. (c) Schematic diagram of multilayer MEA electrolyzer with parallel connection.

(Fig. 9b).[10] In MEA devices, the anode catalysts, AEM and IrO_2 were mixed and pressed into membrane electrodes. The MEA is compressed with a catalyst-loaded GDE, separator membrane (PEM, AEM, or BPM), and anode catalysts for the OER (IrO_2, RuO_2, *etc.*). Pre-treated humidified CO_2 will produce and flow the products out on the same side of the GDE. The single-pass conversion of CO_2 can also be increased through the parallel multilayer MEA device (Fig. 9c). Compared to the traditional flow cell systems, the MEA electrolyzer is a complete battery system, which can achieve a higher ECR current density at a lower voltage. The battery assembled using MEA can obtain separated C_1 and O_2 products, improving the EE and FE of the total battery. The MEA also decreases the distance between both electrodes, reducing ohmic loss and stability degradation caused by significant changes in local pH. The alkaline polymer electrolyte membrane (APEM) device fabricated using special separator membranes can directly use dry CO_2 in the cathode electrolyte to efficiently obtain ECR products. In this electrolyzer, the catalysts should be synthesized on the APEM, accelerating the contact between the CO_2 feedstock and catalytic active sites.[112] The APEM electrolyzer improves the mass transfer and the rate of ion exchange between the two electrolytes. APEM is currently advanced MEA technology, but it is challenging to prepare high-intensity polymer membranes. The synthesis of high-performance SACs can also allow the application of conventional MEA electrolyzers in the large-scale production of C_1 products. Compared to the flow cell, the MEA electrolyzer shows greater stability, reducing the GDE leakage caused by pressure differences. The GDE with superhydrophobic polytetrafluoroethylene could accelerate product diffusion and reduce the HER side-reaction on the working electrode.[113,114] Humified and pressure CO_2 could improve the utilization of the CO_2 feedstock. Multilayer MEA devices can also increase the reaction paths and the single-pass conversion. All these allow ECR to develop from a lab-scale to pilot-plant and even scaled-up process in the future.

5. Techno-economic assessment of C_1 and key indicators for SAC performance

Techno-economic assessment (TEA) is typically used to evaluate the factors that affect the scale of the ECR through systematically analyzing the complete life cycle or half life cycle process of ECR industrialization. There are many considerations for the value of ECR products. From the perspective of energy storage, a higher mass content of hydrogen results in a higher heat of combustion. H_2 is ideal energy but suffers from storage and transportation issues. The U.S. Department of Energy Laboratory proposes that the most valuable reduction product from an energy perspective is methane.[115] Tao's group reported that the ECR products from carbon utilization follow the order of CH_4, formic acid (FA), CO, C_2H_4, EtOH, and MeOH.[116] However, combined with the development of ECR technology, the order of the catalytic performance for the C_1–C_3 products is CO, MeOH, CH_4, FA, ethylene, and acetic acid. The deeply reduced C_1 products methane and methanol are not ideal for scale-up application in industrial ECR, which have lower utilization of electrons ($8e^-$ or $6e^-$ for one molecular product), lower conversion, and the mass yield of CH_4 is only 36%.

In contrast, the mass yield of CH_4 is 105% for FA in the ECR process. Assessment of the separation cost of the product and the sensitivity to market fluctuations shows that the most promising C_1 product in the industrial ECR is CO, followed by FA. Sargent's group summarized the factors that TEA needs to consider from a laboratory perspective,[117] including market size, price of products, battery EE (mainly for C_1 products), chemical efficiency (mainly for C_2 products), electrolyzer cost, operational cost, and separation cost of the whole process. Alternatively, as ECR technology becomes more mature, electricity prices, transportation costs, and CO_2 capture prices have become crucial factors affecting the economic benefits of the ECR industry.[29,118] Establishing an accurate TEA method can predict the possibility of carbon economic development.

5.1. Assessment methods for industrial ECR

Currently, the feasibility methods for evaluating the prospects of the ECR industry include gross-margin analysis and single-variable sensitivity analysis. Paul J. A. Kenis *et al.* used the gross-margin model to analyze the economic feasibility of the ECR. Gross-margin analyzes the ratio of the net benefit generated by the ECR process to this revenue.[29] This value ordinarily should be higher than a fixed value (as shown in Fig. 10, eqn (1), (3), and (4), where the average of the commodity-chemicals

$$\frac{\text{Revenue-cost of goods sold}}{\text{Revenue}} > 0.3 \quad (1)$$

$$\lambda = \lambda_{\text{BOP}} + \lambda_{\text{electrolyzer}} + \lambda_{\text{catalyst}} + \lambda_{\text{electrolyte}} + \lambda_{\text{electricity}} \quad (2)$$

$$\text{Cost of goods sold} = \frac{\lambda}{0.41} + jAt \times 10^{-6} \times \left[VC_{\text{E}} + \frac{36 \sum \text{FE}_{\text{P}} \left(\frac{k_{\text{P}}}{z \times w_{\text{P}}} \right) M}{F} \right] \quad (3)$$

$$\text{Revenue} = \frac{jAt \times 36 \times 10^{-6} \times \sum \frac{\text{FE}_{\text{P}} C_{\text{P}} M}{Z}}{F} \quad (4)$$

Fig. 10 Core equations of the gross-margin model. Reprinted with permission from ref. 29 Copyright 2016, Wiley-VCH.

market is usually 30%). The investment of the whole life cycle includes the cost of the electrolysis cell, balance of the plant, catalyst and electrolyte, and electricity (λ in Fig. 10 eqn (2), all values are state-of-the-art data). The advantage of this assessment method is that the calculation process is relatively simple. Gross-margin analysis is suitable for the rational analysis of a specific catalyst or technology process. However, in many ECR reactions, the current density, EE, FE, and peak and valley electricity prices are all fluctuating parameters, which can hardly be confirmed with specific values. The solution for gross-margin analysis is estimated using average values. Many research groups use single-variable sensitivity analysis to evaluate whether a C_1 product can be profitable within specific parameters. Single-variable sensitivity analysis is more appropriate, given that it does not need to consider all the factors in the whole life cycle. Sargent *et al.* employed this method to analyze the possibility of the one-step ECR industrial production of ethylene, which is hopeless using current technology.[119] When they estimated reducing the CO feedstocks to produce C_2H_4, they were surprised to find this catalytic process has high potential for the industrial production of C_2. Jiao's group performed a sensitivity analysis of the cost to produce C_1 and C_2 in industry (CO, FA, C_2H_4, and EtOH).[120] Through this TEA research, they found the most susceptible cost for the industrial ECR production of CO is the price of electricity, followed by the single-pass conversion rate, which should be higher than 40%. Combined with the increased ohmic loss caused by high voltage, the current density also has a specific range (500–700 mA cm^{-2}). After, the service life cycle of MEA, CO_2 capture price, product price, and FE_{CO} will affect the profits for the CO product in industrial ECR. The most susceptible cost in the industrial ECR production of FA is the current density (200–300 mA cm^{-2}) followed by the price of electricity and the service life cycle of MEA, *etc.* In contrast, the cost of the industrial ECR production of the C_2 products of ethylene and ethanol can still achieve better market values with the state-of-the-art parameters tested with the advanced parallel electrolytic cells and high-efficient catalysts.[111] Sensitivity analysis requires a sizeable statistical database and more calculation models. This TEA method is usually used to estimate the acceptance range of a specific factor affected by other factors (such as product cost and the origin of CO_2) (Fig. 11).

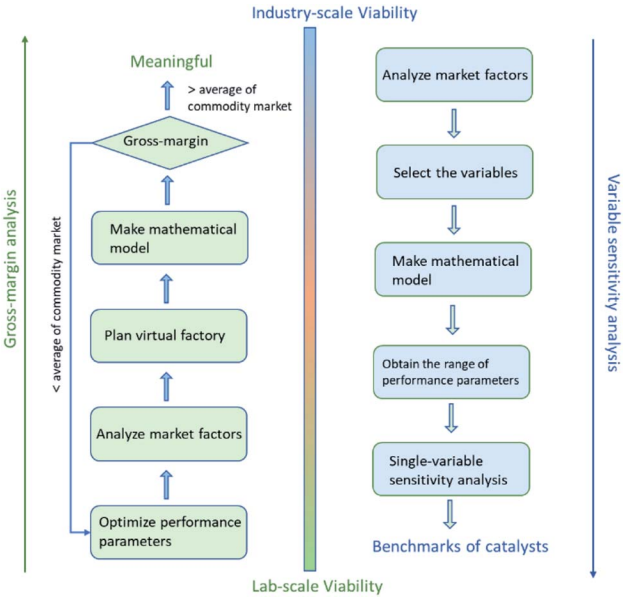

Fig. 11 Different deductive research processes of gross-margin analysis and variable sensitivity analysis: gross-margin analysis can efficiently estimate the specific catalyst with optimized ECR performance. Single-variable sensitivity analysis can estimate the variable range of performance parameters and give the benchmarks for catalysts.

5.2. Technical benchmarks related to ECR industrialization

5.2.1. The benchmarks of plant operating cost and electrolyzer. (1) Peak and valley electricity prices and CO_2 capture techniques affect the cost of industrial ECR. The product value depends on the current floating market price. When estimating the possibility of applying SACs for industrial ECR, we can generally use the peak electricity price and optimized CO_2 capture price (such as \$40 per ton CO_2 and \$0.068 kW h^{-1} electricity in 2017).[116] For reduction products with less electrons (CO) in the ECR, the minimum selling price will be susceptible to the cost of CO_2 capture. Currently, the CO_2 capture cost is low enough to profit from the CO products. (2) Evaluating the economic parameters related to the electrolytic cell is an essential part of the ECR process. The cost of the electrolyzers has gradually decreased after the emergence of series electrolyzers. The MEA electrolyzer is designed to continuously feed CO_2 and efficiently convert it to C_1 with a high current density. However, MEA systems are generally affected by the surface hydrophilization caused by GDE leakage, which results in the side-reaction of the HER occurring. (3) Stability is still an important issue in industrial ECR. Paul J. A. Kenis and others used the gross-margin model to prove that the battery stability time is positively correlated with the ultimate benefit. There is a large coefficient factor.[29] The conventionally used gross-margin model usually requires an ECR conversion of 4000 h to have a 30% net profit in the full lifecycle. However, the typical stability time for lab-scale catalysts is still less than 100 h. (4) Another influence factor consumable is the separator membrane, which is divided into PEM, AEM, and BPM. Different membranes greatly influence the suppression of

crossover problems and the diffusion of anions and organic products. According to the laboratory data statistics, the use of the AEM membrane can decrease the cost of industrial ECR for CO products, and the BPM membrane is more suitable for FA products.

5.2.2. The benchmarks of catalyst performance. Besides adjusting the factors in the ECR electrolyzer, to determine the feasibility of SACs in the ECR, it is necessary to consider the current density, single-pass conversion rate, FE, stabilization time (retaining 90% FE_{C1} stability), EE, and other factors. (1) Although an increase in cell potential is beneficial for the current density and favorable for the yield of C_1, a too high cell potential will increase the cost. Ohmic loss aggravated at high current density reduces the stability of the battery. (2) The single-pass conversion ordinarily needs to be higher than 40% for CO and 80% for FA, which can be solved through parallel electrolyzers and an increase in electrode area for SACs with high FE_{CO} or FE_{FA} close to 100%. (3) In addition to improving the stability in the ECR, reducing the cost of the electrode (IrO_2) and the GDE (catalyst) is also essential to achieving profits. High metal atom utilization of SACs can significantly reduce the cost of catalysts during the whole ECR process. (4) The EE can be promoted by regulating the FE and cell potential. The assessment of the ECR catalytic process shows there are still many challenges for SACs, such as the current density and FE, which are unsuitable for the standard of industrial ECR. The stability should be optimized to decrease the cost of the full lifecycle. Alternatively, industrial ECR is profitable with current SAC research progress in this field.[121,122]

6. Conclusion and outlook

This perspective summarized the methods for the synthesis of SACs with outstanding ECR performances for C_1 products and briefly described the development of electrolyzers. Combining the ECR technical situation and evaluation standard of catalytic performance, we presented the benchmarks in the complete lifecycle of the industrial ECR and summarized the economic feasibility of applying SACs in the industrial electric conversion of CO_2 to C_1 with the guidance of previous techno-economic assessment. Efficient SACs should be designed with appropriate types of metal elements to achieve a higher current density, reduce the concentration of noble metals, facilitate stability during the ECR process, and maintain superhydrophobicity in the alkaline electrolyte. As the conclusion in this perspective, Mn, Fe, Co, Ni, Cd, Ag, and Bi as the active center will produce CO during the ECR process. Also, the single-metal atoms in the main group prefer to produce FA in the ECR. The difference in the electronic structure of the active center caused by the metal species and the atomic coordination environment are the intrinsic factors that affect the ECR reaction. The adsorption energy of CO_2 and various ECR products of the above-mentioned SACs directly affect the selectivity of the ECR process. Carbon-supported SACs have been researched in-depth, but there are still many problems encountered, as follows: (1) the cost of catalyst synthesis; (2) the activity of the catalyst; (3) the uniformity and reproducibility of the catalyst; and (4) the difference in the microscopic atomic structure affect the selectivity of C_1 products.

The main problem of the cost of SACs can be solved by reducing the cost of the substrate. ZIF-8 is a well-known precursor of carbon-supported SACs, which will consume the valuable ligands during the carbonization process. Research on the nitrogen species, the electronic structure of M_1–N–C from ZIF-8, and the effectiveness of residual zinc will help substitute the carbon substrate with low-cost carbon materials. Compared with traditional carbon-supported SACs, nanocrystal/cluster-supported SACs have higher catalytic activity, more uniform microscopic atomic structure, and increased catalytic current density. However, their cost is higher than traditional carbon-supported SACs, which urge researchers to simplify the synthetic process for nanocrystals/clusters. Another crucial problem of SACs is the number of active centers. Densely active centers will improve the conversion and accelerate the catalytic process. The primary method to get dense metal SACs is the "bottom-up" strategy, which assembles small coordination compounds with high concentrations and carbonizes polymers to synthesize dense M–N–C SACs. Correspondingly, the "top-down" strategy may be used more frequently in the future. This indicates the conversion of nanoparticles or high-ordered single-atomic site dispersed metals to coordination-disordered SACs. The research on SACs for the ECR is mainly focused on the H-cell, which is not conducive to scaling-up in industry. Inspired by the development history of electrolyzers, evaluating the ECR performance (current density, FE, cycling stability, and single-pass conversion) of SACs with flow cell or multi-parallel MEA electrolyzers is a crucial step to facilitate the C_1 synthesis scale from lab-scale to pilot-plant.

Under the target of carbon neutrality formulated by each country, the aim is to convert the originally economically unfavorable ECR process to a financially profitable industry due to the decrease in electricity prices and CO_2 capture costs. Without considering the benefits of the policy carbon economy, both the gross-margin model and single-variable sensitivity analysis can be used to evaluate whether the industrial ECR process is profitable. Gross-margin model analysis is a quick and convenient judge for the profitability of a specific catalyst, and this can help analyze the availability of synthesized catalysts. Single-variable sensitivity analysis requires enormous statistical analysis. The deeply reduced C_1 products (CH_4 and CH_3OH) are unfavorable in the entire lifecycle of industrial ECR at the current technicity. Conversely, simple C_1 products (CO and FA) have more potential to yield a profit and realize a net-negative carbon economy. For a specific process, the factors and conditions that generate benefits can be analyzed to help understand the performance indicators that need to be regulated in the catalytic process (Fig. 11). Herein, we also discussed the feasibility of the electrochemical conversion of CO_2 to CO and FA by SACs with guidance from the latest TEA progress. Consequently, some catalytic performance indicators (current density, FE, and EE) need to be optimized in the future.

In conclusion, SACs have improved the relevant catalytic indicators in the industrial ECR economic analysis, which are beneficial due to their high atomic utilization and specific

selectivity of products. Increasingly optimized technology and efficient SACs have facilitated the simple C_1 products (CO, FA) from the laboratory to scaled-up production in the industry. Although relevant factories at the domestic and foreign levels have already developed appropriate industrialized ECR devices, the use of SACs can still further help in process optimization. The three crucial issues are membranes, catalysts, and electrolyzers, which need to be optimized to provide a substantial basis for the industrial conversion of carbon. The era when SACs are used as critical catalysts in the industrial ECR is upcoming.

Conflicts of interest

There are no conflicts to declare.

Acknowledgements

This work was supported by the National Key R&D Program of China (2018YFA0702003), the National Natural Science Foundation of China (21890383, 21871159) and Science and Technology Key Project of Guangdong Province of China (2020B010188002), and the China Postdoctoral Science Foundation (2021M691749, 2020M680505).

Notes and references

1 A. Terando, D. Reidmiller, S. W. Hostetler, J. S. Littell, T. D. Beard, S. R. Weiskopf, J. Belnap and G. S. Plumlee, *USGS Publications Warehouse*, 2020, DOI: DOI: 10.3133/ofr20201058.
2 B. M. Tackett, E. Gomez and J. G. Chen, *Nat. Catal.*, 2019, **2**, 381–386.
3 J. Fu, K. Jiang, X. Qiu, J. Yu and M. Liu, *Mater. Today*, 2020, **32**, 222–243.
4 G. Wang, R. Huang, J. Zhang, J. Mao, D. Wang and Y. Li, *Adv. Mater.*, 2021, e2105904, DOI: 10.1002/adma.202105904.
5 N. M. Haegel, R. Margolis, T. Buonassisi, D. Feldman, A. Froitzheim, R. Garabedian, M. Green, S. Glunz, H.-M. Henning, B. Holder, I. Kaizuka, B. Kroposki, K. Matsubara, S. Niki, K. Sakurai, R. A. Schindler, W. Tumas, E. R. Weber, G. Wilson, M. Woodhouse and S. Kurtz, *Science*, 2017, **356**, 141–143.
6 A. S. Brouwer, M. van den Broek, A. Seebregts and A. Faaij, *Renewable Sustainable Energy Rev.*, 2014, **33**, 443–466.
7 R. J. Budnitz, *Energy Policy*, 2016, **96**, 735–739.
8 Å. Killingtveit, *Future Energy*, 2020, 315–330, DOI: 10.1016/b978-0-08-102886-5.00015-3.
9 C. J. Barnhart, M. Dale, A. R. Brandt and S. M. Benson, *Energy Environ. Sci.*, 2013, **6**, 2804–2810.
10 X. Tan, C. Yu, Y. Ren, S. Cui, W. Li and J. Qiu, *Energy Environ. Sci.*, 2021, **14**, 765–780.
11 Q. Zhu, X. Huang, Y. Zeng, K. Sun, L. Zhou, Y. Liu, L. Luo, S. Tian and X. Sun, *Nanoscale Adv.*, 2021, **3**, 6330–6341.
12 A. Han, Z. Zhang, X. Li, D. Wang and Y. Li, *Small Methods*, 2020, **4**, 2000248.
13 Z. Liu, Y. Du, P. Zhang, Z. Zhuang and D. Wang, *Matter*, 2021, **4**, 3161–3194.
14 Y. Wang, D. Wang and Y. Li, *Adv. Mater.*, 2021, **33**, e2008151.
15 Y. Wang, X. Zheng and D. Wang, *Nano Res.*, 2021, DOI: 10.1007/s12274-021-3794-0.
16 Z. Zhuang, Q. Kang, D. Wang and Y. Li, *Nano Res.*, 2020, **13**, 1856–1866.
17 N. Zhang, X. Zhang, Y. Kang, C. Ye, R. Jin, H. Yan, R. Lin, J. Yang, Q. Xu, Y. Wang, Q. Zhang, L. Gu, L. Liu, W. Song, J. Liu, D. Wang and Y. Li, *Angew. Chem., Int. Ed.*, 2021, **60**, 13388–13393.
18 J. Yang, W. Li, D. Wang and Y. Li, *Small Struct.*, 2020, **2**, 2000051.
19 X. Li, H. Rong, J. Zhang, D. Wang and Y. Li, *Nano Res.*, 2020, **13**, 1842–1855.
20 A. Wang, J. Li and T. Zhang, *Nat. Rev. Chem.*, 2018, **2**, 65–81.
21 X. F. Yang, A. Wang, B. Qiao, J. Li, J. Liu and T. Zhang, *Acc. Chem. Res.*, 2013, **46**, 1740–1748.
22 H. Jing, W. Liu, Z. Zhao, J. Zhang, C. Zhu, Y. Shi, D. Wang and Y. Li, *Nano Energy*, 2021, **89**, 106365.
23 Q. Qu, S. Ji, Y. Chen, D. Wang and Y. Li, *Chem. Sci.*, 2021, **12**, 4201–4215.
24 J. Zhang, W. Cai, F. X. Hu, H. Yang and B. Liu, *Chem. Sci.*, 2021, **12**, 6800–6819.
25 C. M. Gabardo, C. P. O'Brien, J. P. Edwards, C. McCallum, Y. Xu, C.-T. Dinh, J. Li, E. H. Sargent and D. Sinton, *Joule*, 2019, **3**, 2777–2791.
26 A. Liu, M. Gao, X. Ren, F. Meng, Y. Yang, L. Gao, Q. Yang and T. Ma, *J. Mater. Chem. A*, 2020, **8**, 3541–3562.
27 M. Jouny, W. Luc and F. Jiao, *Ind. Eng. Chem. Res.*, 2018, **57**, 2165–2177.
28 K. M. Lee, J. H. Jang, M. Balamurugan, J. E. Kim, Y. I. Jo and K. T. Nam, *Nat. Energy*, 2021, **6**, 733–741.
29 S. Verma, B. Kim, H. R. Jhong, S. Ma and P. J. Kenis, *ChemSusChem*, 2016, **9**, 1972–1979.
30 W. H. Lee, K. Kim, C. Lim, Y.-J. Ko, Y. J. Hwang, B. K. Min, U. Lee and H.-S. Oh, *J. Mater. Chem. A*, 2021, **9**, 16169–16177.
31 G. Meng, J. Zhang, X. Li, D. Wang and Y. Li, *Appl. Phys. Rev.*, 2021, **8**, 021321.
32 X. Zheng, P. Li, S. Dou, W. Sun, H. Pan, D. Wang and Y. Li, *Energy Environ. Sci.*, 2021, **14**, 2809–2858.
33 X. Zhi, A. Vasileff, Y. Zheng, Y. Jiao and S.-Z. Qiao, *Energy Environ. Sci.*, 2021, **14**, 3912–3930.
34 Y. Liu, X. Wu, Z. Li, J. Zhang, S. X. Liu, S. Liu, L. Gu, L. R. Zheng, J. Li, D. Wang and Y. Li, *Nat. Commun.*, 2021, **12**, 4205.
35 Y. Han, J. Dai, R. Xu, W. Ai, L. Zheng, Y. Wang, W. Yan, W. Chen, J. Luo, Q. Liu, D. Wang and Y. Li, *ACS Catal.*, 2021, **11**, 2669–2675.
36 A. Han, X. Wang, K. Tang, Z. Zhang, C. Ye, K. Kong, H. Hu, L. Zheng, P. Jiang, C. Zhao, Q. Zhang, D. Wang and Y. Li, *Angew. Chem., Int. Ed.*, 2021, **60**, 19262–19271.
37 Y. Chen, R. Gao, S. Ji, H. Li, K. Tang, P. Jiang, H. Hu, Z. Zhang, H. Hao, Q. Qu, X. Liang, W. Chen, J. Dong,

D. Wang and Y. Li, *Angew. Chem., Int. Ed.*, 2021, **60**, 3212–3221.
38 X. Sun, Y. Tuo, C. Ye, C. Chen, Q. Lu, G. Li, P. Jiang, S. Chen, P. Zhu, M. Ma, J. Zhang, J. H. Bitter, D. Wang and Y. Li, *Angew. Chem., Int. Ed.*, 2021, **60**, 23614.
39 Z. Zhang, M. Zhou, Y. Chen, S. Liu, H. Wang, J. Zhang, S. Ji, D. Wang and Y. Li, *Sci. China Mater.*, 2021, **64**, 1919–1929.
40 A. Han, X. Zhou, X. Wang, S. Liu, Q. Xiong, Q. Zhang, L. Gu, Z. Zhuang, W. Zhang, F. Li, D. Wang, L. J. Li and Y. Li, *Nat. Commun.*, 2021, **12**, 709.
41 Y. Xiong, W. Sun, Y. Han, P. Xin, X. Zheng, W. Yan, J. Dong, J. Zhang, D. Wang and Y. Li, *Nano Res.*, 2021, **14**, 2418–2423.
42 J. Zhang, Z. Wang, W. Chen, Y. Xiong, W.-C. Cheong, L. Zheng, W. Yan, L. Gu, C. Chen, Q. Peng, P. Hu, D. Wang and Y. Li, *Chem*, 2020, **6**, 725–737.
43 J. Zhang, C. Zheng, M. Zhang, Y. Qiu, Q. Xu, W.-C. Cheong, W. Chen, L. Zheng, L. Gu, Z. Hu, D. Wang and Y. Li, *Nano Res.*, 2020, **13**, 3082–3087.
44 Y. Liu, B. Wang, Q. Fu, W. Liu, Y. Wang, L. Gu, D. Wang and Y. Li, *Angew. Chem., Int. Ed.*, 2021, **60**, 22522–22528.
45 J. Li, P. Pršlja, T. Shinagawa, A. J. Martín Fernández, F. Krumeich, K. Artyushkova, P. Atanassov, A. Zitolo, Y. Zhou, R. García-Muelas, N. López, J. Pérez-Ramírez and F. Jaouen, *ACS Catal.*, 2019, **9**, 10426–10439.
46 L. Jiao, W. Yang, G. Wan, R. Zhang, X. Zheng, H. Zhou, S. H. Yu and H. L. Jiang, *Angew. Chem., Int. Ed.*, 2020, **59**, 20589–20595.
47 Z. Li, Y. Chen, S. Ji, Y. Tang, W. Chen, A. Li, J. Zhao, Y. Xiong, Y. Wu, Y. Gong, T. Yao, W. Liu, L. Zheng, J. Dong, Y. Wang, Z. Zhuang, W. Xing, C. T. He, C. Peng, W. C. Cheong, Q. Li, M. Zhang, Z. Chen, N. Fu, X. Gao, W. Zhu, J. Wan, J. Zhang, L. Gu, S. Wei, P. Hu, J. Luo, J. Li, C. Chen, Q. Peng, X. Duan, Y. Huang, X. M. Chen, D. Wang and Y. Li, *Nat. Chem.*, 2020, **12**, 764–772.
48 Y. Xiong, J. Dong, Z. Q. Huang, P. Xin, W. Chen, Y. Wang, Z. Li, Z. Jin, W. Xing, Z. Zhuang, J. Ye, X. Wei, R. Cao, L. Gu, S. Sun, L. Zhuang, X. Chen, H. Yang, C. Chen, Q. Peng, C. R. Chang, D. Wang and Y. Li, *Nat. Nanotechnol.*, 2020, **15**, 390–397.
49 H. Shang, T. Wang, J. Pei, Z. Jiang, D. Zhou, Y. Wang, H. Li, J. Dong, Z. Zhuang, W. Chen, D. Wang, J. Zhang and Y. Li, *Angew. Chem., Int. Ed.*, 2020, **59**, 22465–22469.
50 B. Xu, H. Wang, W. Wang, L. Gao, S. Li, X. Pan, H. Wang, H. Yang, X. Meng, Q. Wu, L. Zheng, S. Chen, X. Shi, K. Fan, X. Yan and H. Liu, *Angew. Chem., Int. Ed.*, 2019, **58**, 4911–4916.
51 Q. Yang, C. C. Yang, C. H. Lin and H. L. Jiang, *Angew. Chem., Int. Ed.*, 2019, **58**, 3511–3515.
52 N. Mohd Adli, W. Shan, S. Hwang, W. Samarakoon, S. Karakalos, Y. Li, D. A. Cullen, D. Su, Z. Feng, G. Wang and G. Wu, *Angew. Chem., Int. Ed.*, 2021, **60**, 1022–1032.
53 C. Liu, Y. Wu, K. Sun, J. Fang, A. Huang, Y. Pan, W.-C. Cheong, Z. Zhuang, Z. Zhuang, Q. Yuan, H. L. Xin, C. Zhang, J. Zhang, H. Xiao, C. Chen and Y. Li, *Chem*, 2021, **7**, 1297–1307.
54 T. Cui, L. Ma, S. Wang, C. Ye, X. Liang, Z. Zhang, G. Meng, L. Zheng, H. S. Hu, J. Zhang, H. Duan, D. Wang and Y. Li, *J. Am. Chem. Soc.*, 2021, **143**, 9429–9439.
55 J. Feng, H. Gao, L. Zheng, Z. Chen, S. Zeng, C. Jiang, H. Dong, L. Liu, S. Zhang and X. Zhang, *Nat. Commun.*, 2020, **11**, 4341.
56 Y. Pan, R. Lin, Y. Chen, S. Liu, W. Zhu, X. Cao, W. Chen, K. Wu, W. C. Cheong, Y. Wang, L. Zheng, J. Luo, Y. Lin, Y. Liu, C. Liu, J. Li, Q. Lu, X. Chen, D. Wang, Q. Peng, C. Chen and Y. Li, *J. Am. Chem. Soc.*, 2018, **140**, 4218–4221.
57 X. Zhang, Y. Wang, M. Gu, M. Wang, Z. Zhang, W. Pan, Z. Jiang, H. Zheng, M. Lucero, H. Wang, G. E. Sterbinsky, Q. Ma, Y.-G. Wang, Z. Feng, J. Li, H. Dai and Y. Liang, *Nat. Energy*, 2020, **5**, 684–692.
58 S. Wei, A. Li, J. C. Liu, Z. Li, W. Chen, Y. Gong, Q. Zhang, W. C. Cheong, Y. Wang, L. Zheng, H. Xiao, C. Chen, D. Wang, Q. Peng, L. Gu, X. Han, J. Li and Y. Li, *Nat. Nanotechnol.*, 2018, **13**, 856–861.
59 Y. Niu, X. Liu, Y. Wang, S. Zhou, Z. Lv, L. Zhang, W. Shi, Y. Li, W. Zhang, D. S. Su and B. Zhang, *Angew. Chem., Int. Ed.*, 2019, **58**, 4232–4237.
60 A. Han, J. Zhang, W. Sun, W. Chen, S. Zhang, Y. Han, Q. Feng, L. Zheng, L. Gu, C. Chen, Q. Peng, D. Wang and Y. Li, *Nat. Commun.*, 2019, **10**, 3787.
61 J. Jones, H. Xiong, A. T. Delariva, E. J. Peterson and A. K. J. S. Datye, *Science*, 2016, **353**, 150–154.
62 Y. Qu, Z. Li, W. Chen, Y. Lin, T. Yuan, Z. Yang, C. Zhao, J. Wang, C. Zhao, X. Wang, F. Zhou, Z. Zhuang, Y. Wu and Y. Li, *Nat. Catal.*, 2018, **1**, 781–786.
63 J. Yang, Z. Qiu, C. Zhao, W. Wei, W. Chen, Z. Li, Y. Qu, J. Dong, J. Luo, Z. Li and Y. Wu, *Angew. Chem., Int. Ed.*, 2018, **57**, 14095–14100.
64 E. Zhang, T. Wang, K. Yu, J. Liu, W. Chen, A. Li, H. Rong, R. Lin, S. Ji, X. Zheng, Y. Wang, L. Zheng, C. Chen, D. Wang, J. Zhang and Y. Li, *J. Am. Chem. Soc.*, 2019, **141**, 16569–16573.
65 Z. Song, L. Zhang, K. Doyle-Davis, X. Fu, J. L. Luo and X. Sun, *Adv. Energy Mater.*, 2020, **10**, 2001561.
66 G. C. Dubed Bandomo, S. S. Mondal, F. Franco, A. Bucci, V. Martin-Diaconescu, M. A. Ortuño, P. H. van Langevelde, A. Shafir, N. López and J. Lloret-Fillol, *ACS Catal.*, 2021, **11**, 7210–7222.
67 R. Sui, J. Pei, J. Fang, X. Zhang, Y. Zhang, F. Wei, W. Chen, Z. Hu, S. Hu, W. Zhu and Z. Zhuang, *ACS Appl. Mater. Interfaces*, 2021, **13**, 17736–17744.
68 S. Wang, P. Zhou, L. Zhou, F. Lv, Y. Sun, Q. Zhang, L. Gu, H. Yang and S. Guo, *Nano Lett.*, 2021, **21**, 4262–4269.
69 M. Zhang, Z. Zhang, Z. Zhao, H. Huang, D. H. Anjum, D. Wang, J.-h. He and K.-W. Huang, *ACS Catal.*, 2021, 11103–11108, DOI: 10.1021/acscatal.1c02556.
70 J. Lim, P. W. Kang, S. S. Jeon and H. Lee, *J. Mater. Chem. A*, 2020, **8**, 9032–9038.
71 Z. Jiang, T. Wang, J. Pei, H. Shang, D. Zhou, H. Li, J. Dong, Y. Wang, R. Cao, Z. Zhuang, W. Chen, D. Wang, J. Zhang and Y. Li, *Energy Environ. Sci.*, 2020, **13**, 2856–2863.
72 Y. Yao, Z. Huang, P. Xie, L. Wu, L. Ma, T. Li, Z. Pang, M. Jiao, Z. Liang, J. Gao, Y. He, D. J. Kline, M. R. Zachariah, C. Wang,

J. Lu, T. Wu, T. Li, C. Wang, R. Shahbazian-Yassar and L. Hu, *Nat. Nanotechnol.*, 2019, **14**, 851–857.
73 R. T. Hannagan, G. Giannakakis, R. Réocreux, J. Schumann, J. Finzel, Y. Wang, A. Michaelides, P. Deshlahra, P. Christopher, M. Flytzani-Stephanopoulos, M. Stamatakis and E. C. H. Sykes, *Science*, 2021, **372**, 1444–1447.
74 T. Zhang, A. G. Walsh, J. Yu and P. Zhang, *Chem. Soc. Rev.*, 2021, **50**, 569–588.
75 R. T. Hannagan, G. Giannakakis, M. Flytzani-Stephanopoulos and E. C. H. Sykes, *Chem. Rev.*, 2020, **120**, 12044–12088.
76 S. Chen, B. Wang, J. Zhu, L. Wang, H. Ou, Z. Zhang, X. Liang, L. Zheng, L. Zhou, Y.-Q. Su, D. Wang and Y. Li, *Nano Lett.*, 2021, **21**, 7325–7331.
77 J. Yang, W. H. Li, S. Tan, K. Xu, Y. Wang, D. Wang and Y. Li, *Angew. Chem., Int. Ed.*, 2021, **60**, 19085–19091.
78 W. H. Li, J. Yang, H. Jing, J. Zhang, Y. Wang, J. Li, J. Zhao, D. Wang and Y. Li, *J. Am. Chem. Soc.*, 2021, **143**, 15453–15461.
79 X. Xia, Y. Wang, A. Ruditskiy and Y. Xia, *Adv. Mater.*, 2013, **25**, 6313–6333.
80 M. H. Oh, T. Yu, S.-H. Yu, B. Lim, K.-T. Ko, M. G. Willinger, D.-H. Seo, B. Kim, M. Cho, J.-H. Park, K. Kang, Y.-E. Sung, N. Pinna and T. Hyeon, *Science*, 2013, **340**, 964–968.
81 L. Zhanzhao, M. Saruyama, T. Asaka, Y. Tatetsu and T. Teranishi, *Science*, 2021, **373**, 332–337.
82 X. Li, M. Ji, H. Li, H. Wang, M. Xu, H. Rong, J. Wei, J. Liu, J. Liu, W. Chen, C. Zhu, J. Wang and J. Zhang, *Matter*, 2020, **2**, 554–586.
83 L. Jiang, K. Liu, S. F. Hung, L. Zhou, R. Qin, Q. Zhang, P. Liu, L. Gu, H. M. Chen, G. Fu and N. Zheng, *Nat. Nanotechnol.*, 2020, **15**, 848–853.
84 X. Wang, P. Ou, J. Wicks, Y. Xie, Y. Wang, J. Li, J. Tam, D. Ren, J. Y. Howe, Z. Wang, A. Ozden, Y. Z. Finfrock, Y. Xu, Y. Li, A. S. Rasouli, K. Bertens, A. H. Ip, M. Graetzel, D. Sinton and E. H. Sargent, *Nat. Commun.*, 2021, **12**, 3387.
85 R. Shen, W. Chen, Q. Peng, S. Lu, L. Zheng, X. Cao, Y. Wang, W. Zhu, J. Zhang, Z. Zhuang, C. Chen, D. Wang and Y. Li, *Chem*, 2019, **5**, 2099–2110.
86 J. C. Liu, Y. G. Wang and J. Li, *J. Am. Chem. Soc.*, 2017, **139**, 6190–6199.
87 N. Zhang, X. Zhang, L. Tao, P. Jiang, C. Ye, R. Lin, Z. Huang, A. Li, D. Pang, H. Yan, Y. Wang, P. Xu, S. An, Q. Zhang, L. Liu, S. Du, X. Han, D. Wang and Y. Li, *Angew. Chem., Int. Ed.*, 2021, **60**, 6170–6176.
88 X. Shen, X. Liu, S. Wang, T. Chen, W. Zhang, L. Cao, T. Ding, Y. Lin, D. Liu, L. Wang, W. Zhang and T. Yao, *Nano Lett.*, 2021, **21**, 686–692.
89 S. Li, A. V. Nagarajan, D. R. Alfonso, M. Sun, D. R. Kauffman, G. Mpourmpakis and R. Jin, *Angew. Chem., Int. Ed.*, 2021, **60**, 6351–6356.
90 J. Wu, L. Xiong, B. Zhao, M. Liu and L. Huang, *Small Methods*, 2019, **4**, 1900540.
91 T. Li, F. Liu, Y. Tang, L. Li, S. Miao, Y. Su, J. Zhang, J. Huang, H. Sun, M. Haruta, A. Wang, B. Qiao, J. Li and T. Zhang, *Angew. Chem., Int. Ed.*, 2018, **57**, 7795–7799.
92 Y. Xiong, W. Sun, P. Xin, W. Chen, X. Zheng, W. Yan, L. Zheng, J. Dong, J. Zhang, D. Wang and Y. Li, *Adv. Mater.*, 2020, **32**, e2000896.
93 L. Zhao, Y. Zhang, L. B. Huang, X. Z. Liu, Q. H. Zhang, C. He, Z. Y. Wu, L. J. Zhang, J. Wu, W. Yang, L. Gu, J. S. Hu and L. J. Wan, *Nat. Commun.*, 2019, **10**, 1278.
94 X. Nie, M. R. Esopi, M. J. Janik and A. Asthagiri, *Angew. Chem., Int. Ed.*, 2013, **52**, 2459–2462.
95 J. Li, P. Yan, K. Li, J. You, H. Wang, W. Cui, W. Cen, Y. Chu and F. Dong, *J. Mater. Chem. A*, 2019, **7**, 17014–17021.
96 Q. Yang, X. Liu, W. Peng, Y. Zhao, Z. Liu, M. Peng, Y.-R. Lu, T.-S. Chan, X. Xu and Y. Tan, *J. Mater. Chem. A*, 2021, **9**, 3044–3051.
97 T. K. Todorova, M. W. Schreiber and M. Fontecave, *ACS Catal.*, 2019, **10**, 1754–1768.
98 Y. Wang, Z. Chen, P. Han, Y. Du, Z. Gu, X. Xu and G. Zheng, *ACS Catal.*, 2018, **8**, 7113–7119.
99 L. Han, S. Song, M. Liu, S. Yao, Z. Liang, H. Cheng, Z. Ren, W. Liu, R. Lin, G. Qi, X. Liu, Q. Wu, J. Luo and H. L. Xin, *J. Am. Chem. Soc.*, 2020, **142**, 12563–12567.
100 W. Guo, S. Liu, X. Tan, R. Wu, X. Yan, C. Chen, Q. Zhu, L. Zheng, J. Ma, J. Zhang, Y. Huang, X. Sun and B. Han, *Angew. Chem., Int. Ed.*, 2021, **60**, 21979.
101 Y. Wu, Z. Jiang, X. Lu, Y. Liang and H. Wang, *Nature*, 2019, **575**, 639–642.
102 S. Garg, M. Li, A. Z. Weber, L. Ge, L. Li, V. Rudolph, G. Wang and T. E. Rufford, *J. Mater. Chem. A*, 2020, **8**, 1511–1544.
103 J. Huang, F. Li, A. Ozden, A. Sedighian Rasouli, F. P. García de Arquer, S. Liu, S. Zhang, M. Luo, X. Wang, L. Yanwei, Y. Xu, K. Bertens, R. K. Miao, C. T. Dinh, D. Sinton and E. Sargent, *Science*, 2021, **372**, 1074–1078.
104 G. Sahara, H. Kumagai, K. Maeda, N. Kaeffer, V. Artero, M. Higashi, R. Abe and O. Ishitani, *J. Am. Chem. Soc.*, 2016, **138**, 14152–14158.
105 F. Quan, G. Zhan, H. Shang, Y. Huang, F. Jia, L. Zhang and Z. Ai, *Green Chem.*, 2019, **21**, 3256–3262.
106 M. Ramdin, A. R. T. Morrison, M. de Groen, R. van Haperen, R. de Kler, L. J. P. van den Broeke, J. P. M. Trusler, W. de Jong and T. J. H. Vlugt, *Ind. Eng. Chem. Res.*, 2019, **58**, 1834–1847.
107 Y. C. Li, D. Zhou, Z. Yan, R. H. Gonçalves, D. A. Salvatore, C. P. Berlinguette and T. E. Mallouk, *ACS Energy Lett.*, 2016, **1**, 1149–1153.
108 R. S. Jayashree, S. K. Yoon, F. R. Brushett, P. O. Lopez-Montesinos, D. Natarajan, L. J. Markoski and P. J. A. Kenis, *J. Power Sources*, 2010, **195**, 3569–3578.
109 K. P. Kuhl, E. R. Cave, D. N. Abram and T. F. Jaramillo, *Energy Environ. Sci.*, 2012, **5**, 7050–7059.
110 B. Kim, F. Hillman, M. Ariyoshi, S. Fujikawa and P. J. A. Kenis, *J. Power Sources*, 2016, **312**, 192–198.
111 B. Endrodi, E. Kecsenovity, A. Samu, F. Darvas, R. V. Jones, V. Torok, A. Danyi and C. Janáky, *ACS Energy Lett.*, 2019, **4**, 1770–1777.

112 Z. Yin, H. Peng, X. Wei, H. Zhou, J. Gong, M. Huai, L. Xiao, G. Wang, J. Lu and L. Zhuang, *Energy Environ. Sci.*, 2019, **12**, 2455–2462.
113 D. Salvatore and C. P. Berlinguette, *ACS Energy Lett.*, 2019, **5**, 215–220.
114 A. Z. Weber, R. L. Borup, R. M. Darling, P. K. Das, T. J. Dursch, W. Gu, D. Harvey, A. Kusoglu, S. Litster, M. M. Mench, R. Mukundan, J. P. Owejan, J. G. Pharoah, M. Secanell and I. V. Zenyuk, *J. Electrochem. Soc.*, 2014, **161**, F1254–F1299.
115 P. De Luna, C. Hahn, D. Higgins, S. A. Jaffer, T. F. Jaramillo and E. H. Sargent, *Science*, 2019, **364**, eaav3506.
116 Z. Huang, R. G. Grim, J. A. Schaidle and L. Tao, *Energy Environ. Sci.*, 2021, **14**, 3664–3678.
117 M. G. Kibria, J. P. Edwards, C. M. Gabardo, C. T. Dinh, A. Seifitokaldani, D. Sinton and E. H. Sargent, *Adv. Mater.*, 2019, **31**, e1807166.
118 X. Li, P. Anderson, H.-R. M. Jhong, M. Paster, J. F. Stubbins and P. J. A. Kenis, *Energy Fuels*, 2016, **30**, 5980–5989.
119 J. Sisler, S. Khan, A. H. Ip, M. W. Schreiber, S. A. Jaffer, E. R. Bobicki, C.-T. Dinh and E. H. Sargent, *ACS Energy Lett.*, 2021, **6**, 997–1002.
120 H. Shin, K. U. Hansen and F. Jiao, *Nat. Sustain.*, 2021, **4**, 911–919.
121 A. S. Varela, W. Ju, A. Bagger, P. Franco, J. Rossmeisl and P. Strasser, *ACS Catal.*, 2019, **9**, 7270–7284.
122 S. Jin, Z. Hao, K. Zhang, Z. Yan and J. Chen, *Angew. Chem., Int. Ed.*, 2021, **60**, 20627.